High-resolution VUV spectroscopy of H^- in the region near the $H(n=2)$ threshold

P. Balling, H. H. Andersen, C. A. Brodie,* U. V. Pedersen,† V. V. Petrunin,‡ M. K. Raarup, P. Steiner, and T. Andersen
Institute of Physics and Astronomy, University of Aarhus, DK-8000 Aarhus C, Denmark
(Received 23 July 1999; published 5 January 2000)

Experimental investigations of the photodetachment cross section for the negative hydrogen ion in the region near the $H(n=2)$ threshold are discussed. Doppler-tuned spectroscopy in a collinear geometry is used to obtain a comparatively high resolution in this photon-energy range. The ions are accelerated in the ASTRID storage ring, which allows an accurate velocity measurement and further enables the application of momentum-spread reduction techniques. The fixed-frequency vacuum-ultraviolet laser beam (118 nm) is generated by sum-frequency mixing in a xenon gas cell. The photodetachment cross section exhibits pronounced resonances that correspond to the rich spectrum of doubly excited ^1P states near the $H(n=2)$ threshold. The position of the resonances is determined with an accuracy that challenges the current theoretical developments. The experimental observations are used to predict the behavior of a dipole series below $H(n=2)$. The measurement on both hydrogen and deuterium facilitates a study of isotope effects. By means of momentum-spread-reduction techniques it should be possible to resolve the natural linewidth of the narrow dipole resonances. Preliminary studies show that improvements in electron cooling of the H^- beam promise to reach this limit. Finally, the feasibility of extending the high-resolution work to higher-lying ($n=3$) resonances is briefly discussed.

PACS number(s): 32.80.Gc, 39.30.+w

I. INTRODUCTION

Investigations of the neutral hydrogen atom are at the heart of the development of atomic theory. The Coulomb potential is one of the few tractable problems in non relativistic quantum mechanics. It is a remarkable fact that when trying to describe systems with more than a single electron, serious approximations have to be made. Guidance in developing a description of multielectron systems must then come from comparison with experiments. Although the independent electron approximation is generally quite good for systems in singly excited states, the description of multiply excited states is more complicated, since the interaction between two (or more) electrons of similar excitation is strong and their repulsion is poorly described by a single-particle potential. In this case the independent electron approximation may fail even in assigning meaningful quantum numbers to the excited states. In the development of alternative theoretical descriptions of these highly correlated systems, it can be useful to draw on studies of fundamental few-electron systems as, e.g., helium [1].

Over the last 20 years, experimental studies of the negative hydrogen ion have provided a testing ground for the development of the theory of correlated multielectron systems (see, e.g., [2–4] and references therein). Compared to the helium atom, the structure of the negative hydrogen ion is even more strongly influenced by interelectron repulsion, since the nuclear attraction is smaller for this system. In fact, for H^-, the correlation ensures the actual binding of the ground state [5]. Contrary to neutral atoms and positive ions, where the Coulomb tail of the nuclear attraction provides an infinity of bound states, negative ions usually possess just a single bound state. Consequently, negative ion spectroscopy focuses on the determination of positions (and widths/lifetimes) of excited states that are located in the continuum and reveal themselves as resonances, as seen in electron scattering or photodetachment experiments. Generally, the most accurate experimental findings are provided by photodetachment experiments. Since the resonances corresponding to the doubly-excited states are normally located near excited-state thresholds of the neutral system, in order to investigate H^-, one has to overcome the large separation between the ground state and the first excited state of hydrogen. For many years this hindered accurate optical studies of the structure of the system, but in 1977 Bryant and coworkers introduced a technique [6], which for two decades has provided a remarkable amount of spectroscopic information about the negative hydrogen ion [4,6–15].

In the experimental investigations by Bryant *et al.*, the energetic photons were obtained by using standard lasers in the visible and UV range and then upshifting the frequency by as much as 3.4 times by employing the large Doppler shift associated with a high-velocity H^- beam provided by the Los Alamos Meson Physics Facility. The H^- beam-energy was fixed (800 MeV), as was the photon energy of the lasers applied; tunability was achieved by adjusting the angle of intersection between the laser and ion beams. In this way a very large photon energy range could be covered, and this was employed by the New-Mexico group to study the gross behavior of the cross section [9] as well as detailed studies of resonances near the $n=2$ [6,7,9–11], $n=3-4$ [8,14] and $n=5-8$ [12,13] thresholds. The initial observations of the lower-lying resonances were in remarkably good agreement with the calculation by Broad and Reinhardt [16]. The detailed investigations of higher-lying resonances

*Present address: Departments of Physics and Astronomy and Engineering Physics, McMaster University, Hamilton, Ontario, Canada L8S 4M1.
†Present address: Institute for Storage Ring Facilities, University of Aarhus, DK-8000 Aarhus C, Denmark.
‡Permanent address: Physics Department, University of Southern Denmark, Odense, Campusvej 55, DK-5230 Odense M, Denmark.

prompted theoretical investigations of this region [17–19] and again the agreement was good. In addition to the one-photon detachment studies, Bryant *et al.* studied a $^1D^e$ resonance, which was observed in a two-photon detachment experiment [20]. This work was recently extended to investigate isotope shifts [21,22].

The resolution in most of the one-photon studies described above was roughly 8 meV, set by the combined contributions from the momentum spread of the relativistic ion beam and the angular divergence in the crossed-beam geometry. While the technique was extremely versatile and provided a great deal of information about broad resonances, it was clear from comparison with on-going theoretical developments that the narrower features in the cross section could not be resolved. However, a new approach, which improves the resolution in the region near the H($n=2$) threshold has recently been introduced [23,24]. The experimental details will be thoroughly described in Sec. III, where it will be demonstrated that the new technique improved the resolution initially by a factor of ~ 40 due to the application of a collinear geometry and a reduced energy spread of the ion-beam. This resolution allowed a more accurate measurement of the position of a narrow ^1P resonance below the $n=2$ threshold [23] and has now permitted the observation of a second resonance in the dipole series [24], as will be discussed in more detail below.

II. THEORETICAL APPROACHES AND NOMENCLATURE

The Hamiltonian for an atomic system, consisting of a nucleus of charge Z binding N electrons, is the sum of the kinetic energy of each electron, the binding of the electrons in the nuclear potential, the electrostatic repulsion between the electrons, and some additional corrections:

$$H=\sum_{i=1}^{N}\left(\frac{\mathbf{p}_i^2}{2m}-\frac{Ze^2}{r_i}\right)+\sum_{i<j}\frac{e^2}{r_{ij}}+\cdots. \tag{1}$$

The additional terms include relativistic couplings that are generally small for the lighter atomic systems, but which play a decisive role in the final atomic structure (see Sec. IV B for futher detail). When allowing the nucleus to recoil in the center-of-mass frame, there will be a term from the specific mass shift (See Sec. IV C below). Upon omission of these terms, the electrostatic repulsion term is responsible for the need for approximate methods in solving the associated Schrödinger equation. In order to circumvent the nonseparability of this term, the approximation is often made that each electron moves independently in an average field, created by the nucleus and all other electrons. The electrostatic repulsion from the other electrons is approximated by a spherically symmetric one-electron potential, either a model potential or one determined self-consistently, as in the approach of the Hartree-Fock theory. This approximation is traditionally the starting point for most theoretical descriptions of an atomic system and it allows the motion of each electron to be described by a one-electron Schrödinger equation. One can then find one-electron wave functions that are simultaneous eigenfunctions for the effective single-particle Hamiltonian and the orbital and spin angular momentum operators. The single-electron state is described by the two quantum numbers n and l, where n and l are associated with the radial and angular part of the wave function, respectively. The N-electron problem is solved in the basis of (properly antisymmetrized) products of one-electron wave functions, and the set of quantum numbers $n_i l_i$ for all electrons is denoted as the configuration of a particular state.

It is important to notice that the assignment of a configuration to a specific energy level of the atomic Hamiltonian is based on the independent-particle model and the central-field approximation. If the motion of the electrons is strongly coupled, the products of single-particle wave functions are no longer good approximations to the true wave functions. If, however, the correction to the central-field approximation is small, the product wave function gives a good description of a specific state, but the energy associated with a specific configuration splits up due to the electrostatic-repulsion term of the Hamiltonian [Eq. (1)]. Since the Hamiltonian commutes with the total angular momentum and spin operators, one proceeds to form linear combinations of the products of one-electron wave functions such that they become eigenfunctions for these operators as well. In this new coupled basis the Hamiltonian is diagonal within each configuration, and there is just one energy shift for each set of eigenvalues for the total angular and spin angular momenta. The specific eigenvalues are then written as ^{2S+1}L and are denoted as the term for the given configuration. A boon of this method is that the number of possible energy levels for a given configuration can be determined without a calculation of the corresponding energy; the qualitative structure of the system is determined simply from the rules of addition of angular momenta.

The breakdown of the independent-particle approximation is encountered in, e.g., doubly-excited states. One early prominent example was Madden and Codling's photoionization study of He [1], showing only one strong series of resonances as opposed to the two series initially expected. The task of remedying the model by including several configurations in the description of each atomic level (configuration-interaction method) quickly becomes computationally cumbersome. In addition, one must realize that, in this process, any meaning embedded in the original assignment of quantum numbers is lost. In order to avoid this it is necessary to establish another model which is not founded on the independent-particle description, but rather takes as its starting point the correlated motion of the electrons.

In the hypersherical-coordinate description [25,26], new coordinates are introduced for the description of the motion of a two-electron system. A model for two electrons requires six coordinates, for instance the distance from the nucleus to each electron, r_1 and r_2, the angle between the position vectors of the two electrons, θ_{12}, and three Euler angles. In the hyperspherical-coordinate representation, the first two coordinates are replaced with the hyperradius $R=(r_1^2+r_2^2)^{1/2}$, representing the root-mean-square size of the system, and the hyperangle $\alpha=\arctan(r_2/r_1)$ which is a dimensionless quantity related to the radial correlation of the system [2,18,25]. The usefulness of this approach is due to the approximate

separability of the Schrödinger equation in this basis; the equation can be solved for fixed R, and the dependence on this quantity enters through adiabatic potentials, analogous to those arising in the Born-Oppenheimer approximation for molecules. For a given R, the potential energy of the system can be represented by an effective charge, which is a function of α and θ_{12} (see, e.g., [25]).

A resonant state is obtained in a situation where the two electrons are bound to the nucleus, i.e., they remain at finite distance and hence, in the hyperspherical representation, at a finite hyperradius. A resonance can then be described as a state bound in one of the adiabatic hyperspherical potential curves. For large R, the adiabatic potentials converge on those appropriate for the description of one distant electron bound in an induced dipole potential, associated with a neutral-atom threshold of a given main quantum number n. The dipole states are denoted by $m=n+1,n+2,\ldots$, and they satisfy a very definite recurrence relation, as will be discussed in Sec. IV B below. For small R, the potential curves exhibit different behaviors depending on the symmetry of the associated wave functions, normally characterized by the quantum number A. The $A=+$ curves correspond to resonances that have an approximate antinode near the so-called saddle point, $\alpha=45°$, while those with $A=-$ have a node under similar conditions. The $A=+$ and $A=-$ states correspond, respectively, to the electrons being radially in phase or out of phase when approaching the nucleus, as in the symmetric and asymmetric stretch modes, respectively, of a linear tri-atomic molecule. The adiabatic hyperspherical potential curves for the $A=0$ states are generally repulsive for all R and thus hold no bound states. Among the $^1P^0$ curves associated with each neutral atom threshold, there is a single $A=0$ curve while there are $n-1$ curves of $A=+$ and $A=-$ character, respectively. The resonant states supported by a specific potential curve form a series or channel and are labeled according to their symmetry properties. Quite generally, the $A=\pm$ curves have minima that support resonances. The minima of the $A=+$ curves are located at smaller R than those associated with $A=-$. Consequently, the $A=+$ resonances are excited more easily from the ground state than the $A=-$ resonances, since the wave functions of the $A=+$ resonant states more closely resemble the localized ground state wave function. In the lowest level of a given channel of the $A=+$ type (denoted by $m=n$), the two electrons spend considerable time at a comparable distance to the nucleus. They interact strongly and the state is thus quite unstable, resulting in rapid autodetachment. For higher-lying resonances in the channel (i.e., for a given $A=+$ curve), the states labeled by $m=n+1,n+2,\ldots$, form a series of resonances converging on the associated threshold that become increasingly dipole-like. A resonance associated with an $A=-$ curve can be roughly characterized by one electron being fairly distant from the excited, neutral hydrogen atom. The interaction between the electrons is weak, primarily through the induced dipole moment, and accordingly, the resonance is more stable against autodetachment. There is again an infinity of resonances, $m=n+1,n+2,\ldots$, converging on the neutral-atom threshold, corresponding to an infinite dipole series. It is tempting to loosely speak of n and m as the principal quantum numbers of the inner and outer electrons, respectively [19], a misleading nomenclature since the different m-states contain contributions from a large number of hydrogenlike configurations [27].

An obvious consequence of the strong correlation in the doubly excited states under consideration is the inadequacy of the one-electron angular momenta quantum numbers. Instead, Herrick and Sinanoglu have suggested the introduction of (K,T) quantum numbers as collective quantum numbers that describe angular correlation [28,29]. K is proportional to the average $\langle r_< \cos\theta_{12}\rangle$, where $r_<$ is the distance to the inner electron [2]. The T quantum number can be interpreted as the projection of $\mathbf{L}$ onto the axis $\mathbf{r}_1-\mathbf{r}_2$. These quantum numbers are used to label the different hyperspherical potential curves discussed above, i.e., they specify the different channels. A resonance of parity π can thus be described by the symbol ${}_n(K,T)^A_m\,{}^{2S+1}L^\pi$, where the last part denotes the usual term. This notation, in fact, carries redundant information, since $A=\pi(-1)^{S+T}$. We will here use the slightly more compact notation ${}_n\{\nu\}^A_m\,{}^{2S+1}L^\pi$, where $\nu=\frac{1}{2}(n-1-K-T)$ is the bending vibrational quantum number of the three-body rotor (compare again to the linear tri-atomic molecule), i.e., it is the number of nodes in θ_{12} [17].

Sadeghpour and Greene [17] and Sadeghpour [18] have calculated the adiabatic hyperspherical potential curves for highly excited states of H^- converging on neutral-atom thresholds below $n=12$. By this means, they have ascribed quantum numbers to resonances observed in the photodetachment experiments mentioned above [8,12–14]. They note the propensity rule that all the observed resonances have $\nu=0$, i.e., only zero point motion in the bending mode. Furthermore, the experiments have only revealed resonances associated with the lowest-lying $A=+$ curve within each manifold of the $2n-1$ curves converging on a specific neutral-atom threshold, n [17]. The only exception to this rule has been the so-called Feshbach resonance below $n=2$ (${}_2\{0\}^-_3$ in the present notation), which was the only observed $A=-$ resonance. The hyperspherical approach is only just beginning to compete with other methods in the attempt to provide quantitative comparison with experimental cross sections. Consequently, the authors of Refs. [17] and [18] have in a different investigation [19] used an R-matrix calculation to perform an accurate calculation of the photodetachment cross section for H^-. Ho [30] used complex rotation to obtain resonance parameters for the ${}_2\{0\}^-_3$ resonance. Tang *et al.* [31] used a close-coupling method in terms of hyperspherical coordinates to study partial and total photodetachment cross sections of H^-. Lindroth *et al.* [27,32,33] performed complex-rotation calculations to examine the narrow ${}_2\{0\}^-_m$ resonances below $n=2$. The importance of relativistic effects for the dipole series has been discussed extensively by the Friedrich group [34,35]. A saddle-point–complex-rotation approach was used by Chen [36], while Gien [37] used the Harris-Nesbet variational method. In a recent paper by Kuan *et al.* [38], the results of a complex-rotation calculation are directly compared with the published experimental results [24], demonstrating an excellent agreement. As evidenced above, the theoretical activ-

ity on the H^- ion is very high. It seems reasonable to assert that the system provides a test ground for the development of theoretical approaches.

To summarize this section, quantitative calculations as well as models providing an efficient taxonomy are important in the understanding of electron correlation. For H^-, the hyperspherical approach seems a useful framework for the assignment of correlation quantum numbers, while a number of accurate calculational methods compete to provide the most accurate resonance parameters.

III. EXPERIMENTAL APPROACH

A. Generation of vacuum-ultraviolet light

A spectroscopic study of the doubly-excited states in H^- requires access to the vacuum-ultraviolet (VUV) region of the spectrum, accomplished in the present study by nonlinear conversion techniques. When short wavelengths are involved, the nonlinear techniques generally utilize gaseous media since no suitable crystal materials are available below $\sim$190 nm. These methods are becoming increasingly important in many areas of physics and chemistry. By combining various gases and metal-vapors with selected laser wavelengths, it is possible to use four-wave mixing to cover the VUV region down to $\sim$110 nm [39]. Third-harmonic generation is the special case of just a single driving laser and it has the benefits of technical simplicity and—very importantly—the potential of obtaining very narrow linewidth radiation with reasonable efforts.

The third-harmonic field of the 355 nm output from a neodymium-doped yttrium aluminum garnet (Nd:YAlG) laser, 118 nm, happens to be located at a slightly higher photon energy than the $5p$-$5d$ transition in Xe. As a consequence, the refractive index of a Xe gas at this wavelength is lower than that at 355 nm. This is important in order to obtain phase-matching for the third-harmonic process: The optical field at the third harmonic frequency consists of two parts, a free wave that propagates with the usual phase velocity for this frequency, and a driven wave that propagates with the phase velocity of the driving field. In general, these two phase velocities are different due to the different refractive indices at the driving and harmonic frequencies. This means that the free and the driven component of the harmonic field will interfere constructively or destructively in different parts of the nonlinear medium, thus resulting in a much reduced production efficiency. In order to obtain a reasonable conversion, it is necessary to adjust the phase mismatch between the two waves. For plane waves, phase matching is achieved for zero wave-vector mismatch, $\Delta k=0$, as is expected also from energy- and momentum-conservation requirements. In a focussed geometry, if the driving field is a Gaussian beam of Rayleigh length, z_0, much smaller than the length of the gas cell, the wave-vector mismatch must satisfy $z_0\Delta k=-1$ [40,41]. There are several ways to obtain phase matching, but a very efficient method over restricted regions of the spectrum is applying gas mixtures. In order to be able to adjust the wave vector mismatch, it is necessary that one of the components has negative dispersion, while another has positive dispersion. This can be obtained with a mixture of Xe and Ar, as first demonstrated by Kung *et al.* [42] and later applied by several groups (see Ref. [39] and references therein).

In fact, the required phase matching with a focussed beam can also be obtained with just a single gas component with negative dispersion, given the proper combination of Rayleigh length and pressure. The wave vector mismatch for Xe in 355 to 118 nm conversion has been calculated to be -6.12×10^{-17} cm^2 per atom [43], which means that for a fixed Rayleigh length, $\sim$0.1 cm in our case, a pressure of 7 mB (at room temperature) is needed to obtain phase matching. In the present experiment, this approach gave the maximum production efficiency at high input power levels. Of course, the low pressure leads to a relatively small density of atoms that serve as the source for the third-harmonic field, but at high input powers the conversion efficiency becomes limited by non-linear changes in the refractive index (Kerr effect) that destroy the phase-matching condition [44]; this unwanted effect is suppressed by using a low pressure.

Under typical experimental conditions a 160 mJ 355 nm laser pulse of $\sim$8 ns duration is focussed to a $\sim$20-μm-diameter focus, corresponding to an intensity of 5×10^{12} W/cm^2. With these conditions approximately 10^{11} VUV photons per pulse are generated, corresponding to a quantum conversion efficiency of $\sim3\times10^{-7}$. The number of 118 nm photons is measured absolutely by integrating the number of generated photoions in an NO ionization cell [45]. The VUV light is separated from the 355 nm driving field by a focussing grating of MgF_2 coated aluminum, 1200-lines-per-mm ruling and 498-mm radius of curvature. The grating leads to astigmatic focussing of the VUV laser beam. This is compensated by recollimating the light with a curved mirror of an appropriate radius of curvature and angle of incidence at a specific distance from the grating. The combined effect of the grating and the mirror is the formation of an approximately parallel VUV beam of slightly elliptic cross section. The astigmatic focussing of the VUV beam is a necessary consequence of using a curved grating, but it allows for efficient blocking of scattered 355 nm light through the application of slits in the vertical and horizontal foci of the beam. The generated beam propagates through a LiF window to the ultrahigh-vacuum conditions of the storage ring and provides $\sim10^{10}$ photons per pulse in a $\sim$1 cm^2 beam to be used in the experiment (see the following section). After the interaction region inside the storage ring an electron-multiplier plate with a fluorescent screen is used to visualize the location and spatial profile of the VUV laser beam.

When applying VUV light for spectroscopic purposes, as in the present context, it is important that the generated light has a narrow bandwidth. In the general four-wave-mixing scheme it is very demanding to make the pulsed light transform limited. However, in the case of a single driving laser this is feasible. In particular, since we rely on converting the output from a Nd:YAlG laser, a narrow bandwidth can be obtained simply by using an injection seeded laser. The laser applied has a specified bandwidth <0.4 μeV and the nonlinear conversion is not expected to add to this significantly [41], which means that this contribution to the resolution is more than two orders of magnitude below the present limit in

the experiment, see below. The absolute photon energy is measured (at the second-harmonic output from the laser) by comparison to the output from a tunable dye-laser in this wavelength region. The dye-laser can be scanned through various well-known transitions in opto-galvanic lamps and the wavelength of the Nd:YAlG laser can be determined by comparison in interferometers. The resulting photon energy of the VUV light is 10.48299(2) eV.

B. Doppler-tuned spectroscopy

Due to the Doppler effect, an ion in motion sees an effective photon energy that differs from the laboratory photon energy. In Doppler-tuned spectroscopy this is utilized as a tool to perform spectroscopy with photons of fixed energy. If θ denotes the angle of incidence on the ion beam with $\theta = 0°$ being a head-on collision, v is the velocity of the ion beam, and $\hbar\omega_0$ is the laboratory photon energy then the effective photon energy is

$$\hbar\omega = \hbar\omega_0\gamma\left(1+\frac{v}{c}\cos\theta\right), \tag{2}$$

where $\gamma=(1-v^2/c^2)^{-1/2}$ is the Lorentz factor. From the equation above it is obvious that there are three contributions to the resolution in the effective photon energy: angular divergence, ion-velocity spread and bandwidth of the light source. The last contribution can be eliminated by the application of narrow-bandwidth sources as described in section III A. The contribution from angular divergence is

$$\Delta(\hbar\omega) = \hbar\omega_0\gamma\frac{v}{c}\sin\theta\,\Delta\theta. \tag{3}$$

Obviously, by choosing an angle of intersection close to 0° (or 180°) the influence of this term can be reduced tremendously [46]. In our setup $\theta = 0.6°$ and using an estimate of $\Delta\theta = 0.2°$ this term contributes 18 μeV (FWHM) to the spread for a $\sim$1 MeV H^- beam. It turns out that the momentum spread contributes most to the resolution. We have

$$\Delta(\hbar\omega) = \hbar\omega_0\left(1+\frac{c}{v}\cos\theta\right)\frac{\Delta E}{Mc^2}, \tag{4}$$

where M is the mass of the ion and ΔE the spread in kinetic energy. For many radio-frequency based accelerators, the energy-definition, $\Delta E/E$, is roughly constant at different energies. If this is the case, the contribution to the resolution from the momentum spread, Eq. (4), grows roughly as the square root of the beam energy for low energies. This will be important for the possible extension of the present work to higher-lying resonances (see Sec. IV D). At the $\sim$1 MeV needed for the present investigation, the contribution for $\Delta E/E = 7\times10^{-4}$ is 180 μeV. This limiting factor to the resolution can be reduced by applying momentum-spread-reduction techniques (see Sec. IV D).

The experiment is performed at the Aarhus Storage Ring Denmark (ASTRID) [47]. Negative hydrogen ions (H^- or, alternatively, D^-) are produced in a duo-plasmatron ion source, accelerated to 150 keV, mass analyzed and injected into the storage ring. Following injection, the ion beam is accelerated to $\sim$1 MeV(H^-) by a radio-frequency field, which is subsequently turned off. Along one of the straight sections of the ring ($\sim$8 m long, see Fig. 1), the ions are overlapped with the counter-propagating VUV laser beam (Sec. III A). The ions are photodetached with a probability $P=\sigma N/A_{vuv}$, where σ is the cross section and N/A_{vuv} $\sim10^{10}$ cm^{-2} is the number of photons per pulse per beam area. A typical off-resonant cross section in the photon energy region under investigation is 10 Mbarn [32], which gives a detachment probability of $P_{nr}=10^{-7}$. Right after acceleration, the circulating current is typically 0.5μA, corresponding to $\sim$0.2 photo-induced neutral atoms per laser pulse. (At the peak of the strongest resonance this number is roughly 50 times larger with the present resolution). The neutral atoms pass undeflected through the magnetic lattice of the storage ring and impinge on an electron-multiplier-plate detector located after the bending magnet. Due to the finite size of the detector (25×25 mm^2) and the (albeit small) angular spread of the ion-beam, an estimate of only $\sim$10% of the neutrals hit the detector. Furthermore, the measured signal contains contributions from both the photodetachment process and collisional processes. The signal is counted over a short time interval (gate) after each laser pulse (covering the flight times for the ions that interacted with the laser light, $\sim$700 ns). In the relevant time interval, the collisional background is typically $\sim$40% of the off-resonant photoinduced signal. In order to determine this contribution, the pure collisional signal is measured in a separate (delayed) time interval. Due to its low duty-cycle, the laser hardly affects the total number of ions in the storage ring; the decrease in the circulating current is determined by the col-

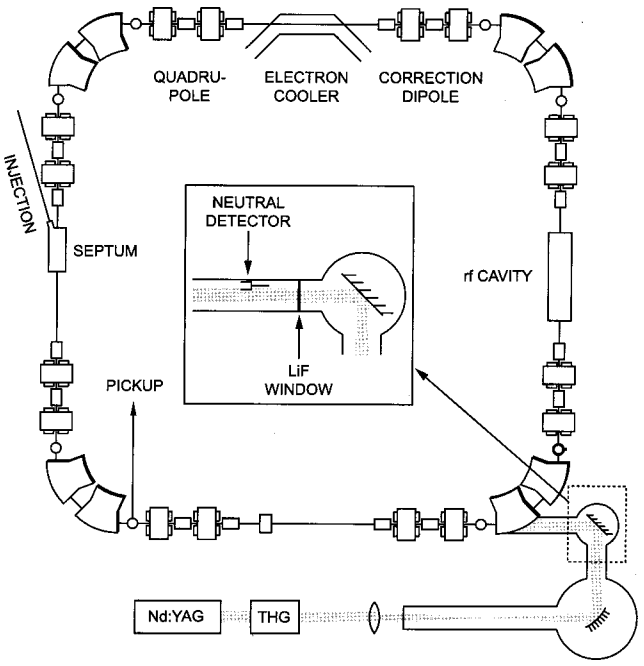

FIG. 1. A schematic of the experimental setup showing the VUV laser system and the ASTRID storage ring with injector, acceleration section, and detection system.

lisionally limited storage time of a few seconds. Since the gated counts are measured versus time after acceleration, they reflect this exponential decay. The relative photodetachment cross section is reflected in variations in the preexponential factor for the photoinduced signal at the different effective photon energies (i.e., different ion-beam energies). In order to normalize the photo signal to the number of ions in the ring, we always take the ratio to the preexponential factor for the pure collisional decay and divide by the decay time to account for possible changes in vacuum conditions in the ring that will change the collisional probability. Normalization to the photon flux is performed by measuring the amount of charge on the detector for the VUV light (also used for visualization of the beam, see Sec. III A) after each laser pulse and recording the running average. The acceleration sequence for the storage ring reduces the duty cycle significantly; the injection and subsequent acceleration of the ion-beam involves the ramping of magnets in the ring and can only be repeated every ~ 30 sec. During the subsequent exponential decay, the laser light (at 10 Hz repetition rate) typically generates 0.5–25 photoinduced neutral atoms (nonresonant/resonant cross section).

Since the effective photon energy is determined by the Doppler shift, an accurate measurement of the ion velocity is very important. For storage-ring experiments this can be done by measuring the revolution frequency of the ions in the ring, assuming a well-known circumference. The revolution frequency is measured by a so-called Schottky pick-up, which relies on the detection of statistical density fluctuations (Schottky noise) of the discrete charges in the beam. The frequency spectrum is peaked at the different harmonics of the revolution frequency and the width is determined by the distribution of frequencies (i.e., velocities) in the beam. While counting the neutral-atom production for a given ion-beam energy, the Schottky spectrum for a specific harmonic of the revolution frequency is averaged on a spectrum analyzer. The resulting spectrum is fitted well by a Gaussian function and the center frequency is used to determine the velocity while the width provides information about the velocity-spread of the ions (see also Sec. IV D). With this procedure the frequency can be determined with an accuracy limited only by the width of the peaks, which means that the experiment is very sensitive to changes in velocity. This is important because changes in velocity correspond to changes in effective photon energy. Assuming an accuracy of 10% of the width leads to a contribution of only 16 μeV to the photon energy resolution. The disadvantage of the above measurement technique is related to the difficulty in providing an absolute velocity measurement. The reason is that this procedure has to rely on knowledge of the exact circumference of the storage ring (or rather the orbit length). ASTRID is designed for an ideal orbit length of 40 m, and the most accurate calibration of this number is obtained by the fact that the storage ring can also store a relativistic electron beam. In this case the velocity of the particles is very well defined (essentially the velocity of light) and the orbit length can be very accurately determined from the measured revolution frequency. These observations give a circumference of 39.993(1) m [48]. The orbit length can change by small amounts for different settings of the ring. However, the position of the stored beams can be measured by position pick-ups distributed in the ring. If we assume that the beams are located at the same position to better than ± 10 mm, a conservative estimate for the accuracy of the beam position measurements, then the corresponding uncertainty in the orbit length is ± 8 mm, as can be calculated from the dispersion of the ASTRID storage ring [47]. By additionally incorporating an estimate of potential systematic effects (as, e.g., closed-orbit corrections [48]), a 39.99(2) m circumference for the ions is assumed. This contributes 0.2 meV to the uncertainty in the effective photon energy. In all of the measurements this is the main uncertainty in the absolute energy measurements, while relative energies are determined roughly one order of magnitude better than this.

IV. RESULTS AND DISCUSSION

A. Observed structures

Figure 2 shows the measured relative photodetachment cross section for D^- as reported initially in Ref. [24]. The two narrow resonances are the ${}_2\{0\}_3^-$ and the ${}_2\{0\}_4^-$ resonances, respectively (or ${}_2(1,0)_3^-$ and ${}_2(1,0)_4^-$ in the K,T notation). These are the first two members of an $A=-$ series, which has strong dipole character, see Sec. IV B. The broad resonance above the $n=2$ threshold (at 10.956 eV) is the ${}_2\{0\}_2^+$ (or ${}_2(0,1)_2^+$) resonance, which is the single resonance of $A=+$ character associated with $n=2$. These three resonances were observed for both H^- and D^-. The photodetachment cross section in the vicinity of the narrow resonances is well described by a Fano parametrization [32],

$$\sigma(\hbar\omega)=\sigma_0\frac{(q+\epsilon)^2}{1+\epsilon^2}, \tag{5}$$

where $\epsilon=2(\hbar\omega-E_{res})/\Gamma$. E_{res}, Γ, and q are the energy, width and asymmetry parameter of the resonance, respectively. As seen from the expanded views of the ${}_2\{0\}_3^-$ and ${}_2\{0\}_4^-$ resonances in Figs. 2(b) and 2(c), the observed widths are significantly larger than the 30-65 μeV (${}_2\{0\}_3^-$) and ~ 2 μeV (${}_2\{0\}_4^-$) predicted by theory [27,31,36,37]. This reflects the resolution of the present experiment and, as discussed in section III B above, is mainly due to the velocity spread of the ion beam in the storage ring. Due to the very small width of the ${}_2\{0\}_4^-$ resonance, its observed shape is completely dominated by this Doppler broadening, and hence a fit to a Gaussian form is chosen. Resonance positions of 10.9519(2) eV (H^-) and 10.9553(2) eV (D^-) are obtained. The observed width of ~ 180 μeV (FWHM) is entirely consistent with the relative velocity spread of $\sim 4\cdot 10^{-4}$ determined from the Schottky spectrum of the stored ion beam (see Sec. III B), which is an immediate consequence of Eq. 2 (in the nonrelativistic limit). The true width of the ${}_2\{0\}_3^-$ resonance is also smaller than the present resolution, but the asymmetry of the cross section is clearly visible in the tails of the observed profile. Consequently, the analysis of this structure has to rely on a comparison with a convolution of the cross section profile, Eq. (5), and the dis-

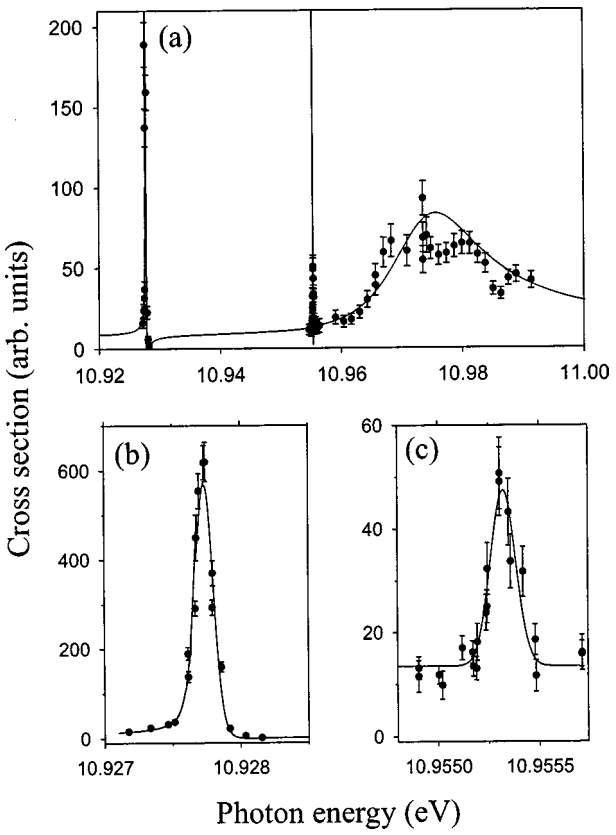

FIG. 2. Relative photodetachment cross section (measured neutral atom yield corrected for collisional background) vs. effective photon energy. The error bars indicate a statistical uncertainty of one standard deviation. (a) The full energy range. The data have been normalized to the theoretical results of Lindroth [32] (solid curve). Some of the measured points on the $_2\{0\}_3^-$ resonance at 10.9277 eV exceed the vertical scale of the plot. (b) Blow-up of the region near the $_2\{0\}_3^-$ resonance. The solid curve shows a fit to a Fano profile convolved with the photon energy resolution as discussed in the text. (c) Blow-up of the region near the $_2\{0\}_4^-$ resonance. The solid curve shows a fit to a Gaussian profile.

tribution of effective photon energies due to the velocity spread [cf. Eq. (4)]. The resulting resonance positions of 10.9243(2) eV and 10.9277(2) eV for H^- and D^- are, within the quoted uncertainties, independent of the other parameters of the fit. The measured cross section also constrains the Γ and q parameters: Values outside the ranges listed in Table I lead to a systematic deviation from the data. Table I gives a comparison between the present results and previous experimental and recent theoretical values. In order to improve the determination of the width and asymmetry parameters for the resonance, it is necessary to improve the resolution of the experiment. This can be done by reducing the momentum-spread of the ion beam, as will be discussed in more detail in Sec. IV D.

The agreement with our previously reported position for the $_2\{0\}_3^-$ resonance is excellent [23]. Both of our results deviate from the former experimental result [11]. The discrepancy may be attributed to an incorrect calibration of the effective photon energy (i.e., of the angle of intersection) in the New Mexico experiment; due to experimental limitations, the calibration had to rely on a transition to $n \geqslant 4$ in hydrogen, which corresponds to a change in photon energy of 17% from the position of the resonance. This change is almost three orders of magnitude larger than the present discrepancy. The above assumption is supported by the observation that the position of the $_2\{0\}_2^+$ resonance exhibits a similar deviation from the calculated position [32]. The recent calculations all agree well with the present experimental values. The initial report of our data [24] has initiated a renewed interest in this photon-energy region, since the comparatively high accuracy allows for a critical test of the numerical accuracy of calculations. In addition, the question of the number of resonances expected in the dipole series has received significant attention, as discussed in Sec. IV B below. The present data for the $_2\{0\}_2^+$ shape resonance do not allow an accurate evaluation of its resonance parameters. The fluctuations in the measured cross section are attributed to variations in the overlap due to changes in the ion-beam trajectories over the very large range of ion storage energies required to cover the $_2\{0\}_2^+$ resonance. It is important to note that similar effects do not play a role when scanning small effective-photon-energy ranges. For instance, the total range of beam energies needed to cover each of the narrow resonances is only $\sim 10^{-3}$ of the total beam energy, while it is ~ 0.2 for the broad resonance. The experimental points in Fig. 2(a) only serve to indicate that the measured cross section is consistent with theoretical predictions [32].

B. $_2\{0\}_m^-\,{}^1P^0$ dipole series

The specific properties of atomic hydrogen lead to a degeneracy of different angular momentum states for the excited states and therefore the existence of the linear Stark effect for this atom. An immediate consequence of this phenomenon is the fact that excited hydrogen states in an electric field can possess a permanent electric dipole moment. The resulting potential, the dipole potential, has the distinct $1/r^2$ character. Considering, specifically, an electron approaching a hydrogen atom excited to $n=2$, the electric field from the distant electron will polarize the atom and the incoming electron will feel a potential, which consists of a repulsive centrifugal term and an attractive dipole potential, both of which behave as $1/r^2$. Depending on the relative strength of the two terms, the electron may or may not be bound to the excited state. This problem was first treated by Gailitis and Damburg [49]. They showed that a Hamiltonian of the form

$$H = -\frac{d^2}{dr^2} + \frac{l(l+1)+\alpha}{r^2}, \tag{6}$$

where α is the strength of the dipole potential, may lead to an infinite series of bound states. If, among the eigenvalues for $l(l+1)+\alpha$, there exists one, a, which is smaller than $-1/4$, then the cross section exhibits strong variations corresponding to an infinite series of resonances converging to the excited-state threshold. The infinite series satisfies an inter-

TABLE I. A comparison of experimental and theoretical results for the $^1P^o$ resonances of H^- and D^- converging to the $n=2$ threshold.

	$E_R(H^-)$ / eV	$E_R(D^-)$ / eV	Γ / μeV	q
$_2\{0\}_3^{-}\,{}^1P^o$				
Experiment				
MacArthur *et al.* [11]	10.9264(6)			
Balling *et al.* [23]	10.9243(3)			
Andersen *et al.* [24] and present	10.9243(2)	10.9277(2)	$20<\Gamma<60$	$-30<q<-10$
Present [a]			57(15)	
Theory				
Ho [30] [b]	10.9245	10.9277	35.9	
Sadeghpour *et al.* [19] [b]	10.9255	10.9287	28.8	
Tang *et al.* [31] [b]	10.924	10.927	65.3	
Lindroth *et al.* [27] [b]	10.9245	10.9277	37.2	-16.5
Chen [36] [b]	10.92452	10.92774	35.6	
Gien [37] [c]	10.92450	10.92772	37.7	
Bürgers [33] [b]	10.92452	10.92774	37.2	
Kuan *et al.* [38] [b]	10.92452	10.92774	36.9	
$_2\{0\}_4^{-}\,{}^1P^o$				
Experiment				
Andersen *et al.* [24] and present	10.9519(2)	10.9553(2)		
Theory				
Tang *et al.* [31] [b]	10.952	10.955		
Lindroth *et al.* [27] [b]	10.9521	10.9553	2	-11
Chen [36] [b]	10.95213	10.95535	1.9	
Gien [37] [c]	10.95198	10.95521	2.0	
Bürgers [33] [b]	10.95212	10.95534	2.1	
Kuan *et al.* [38] [b]	10.95208	10.95530	1.8(2)	

[a]Preliminary. Data are obtained by the application of electron cooling and the width fitted by deconvolving the measured velocity distribution, see text.

[b]Converted from the total energy of the system (in a.u.) to the energy with respect to the ground state using 1 a.u.$=27.2113962M/(M+m)$ eV. Ground-state energies of 14.35265 eV (H^-) and 14.35680 eV (D^-) are derived from Ref. [51] neglecting the small mass dependence of the relativistic and QED corrections.

[c]Converted from transition energies in Rydberg by applying 1 Ry = 1 a.u./2, as defined in the previous tablenote.

esting recurrence relation: both the binding energy of the states and their width become exponentially smaller going up the series:

$$\frac{\epsilon_m}{\epsilon_{m+1}}=\frac{\Gamma_m}{\Gamma_{m+1}}=R=\exp\left(\frac{2\pi}{\sqrt{-1/4-a}}\right), \tag{7}$$

where ϵ is the energy relative to the threshold. It is possible to relate the eigenvalues of $l(l+1)+\alpha$ to a specific channel in the collective quantum numbers; Herrick [50] offers a perturbative expression for the eigenvalues in terms of K and T. Specifically, near the $n=2$ threshold of hydrogen, the values of $a, -3.71$ (from $3-3\sqrt{5}$) and 2, as calculated already by Gailitis and Damburg [49], have been shown to correspond to the $_2\{0\}_m^-$ and the $_2\{0\}_m^+$ series, respectively. This means that only the $A=-$ channel will exhibit resonances, while for the $A=+$ channel, the attraction is too weak to form a dipole series. The short-range attraction in the $A=+$ channel is, however, strong enough to facilitate a single resonance above the threshold, $_2\{0\}_2^+$. Using $a=-3.71$, one obtains [Eq. (7)] $R=29.334$. The ratio determined in the present experiment, 26 ± 5, is quite consistent with this number. This may appear surprising, since the electronic potential deviates significantly from the pure dipole behavior in the inner region for the $A=-$ channel. The agreement will be good, however, if the electron is exposed primarily to the outer dipole tail of the potential, which is an increasingly good approximation as m increases. In fact, the calculated average radial distances of the most distant electron are as large as 34 a.u. and 187 a.u. for the $_2\{0\}_3^-$ and $_2\{0\}_4^-$ states, respectively [27]. The present observations of the $_2\{0\}_3^-$ and $_2\{0\}_4^-$ resonances can be used to predict the position of the next member in the series, $_2\{0\}_5^-$. It should be located about 40 μeV below the H($n=2$) threshold. This energy is, however, comparable to the fine-structure splitting of the H($2p$) state of the neutral atom, and thus one can no longer neglect the effect of the relativistic interaction and QED effects. The proper inclusion of these terms leads to a lifting of the de-

generacy, destroying the dipole potential. This problem has been studied in detail theoretically by Lindroth *et al.* [27] and by Purr *et al.* [34,35]. They conclude that the $A=-$ resonance series is terminated after the third member, and that this third ${}_2\{0\}_5^-$ state is shifted significantly closer to threshold and should be found only 19 μeV below the H($2p_{1/2}$) state, with a width of just 0.06 μeV. In addition, the authors of Ref. [35] have shown that a high-lying member of the ${}^3P^0$ series contains a significant admixture (17%) of ${}^1P$ character and thus is—in principle—amenable to optical studies.

C. Isotope effects

The ability to perform the present experiment with both H^- and D^- allows for an investigation of isotope effects. In addition, the very narrow structures under investigation in the present study may permit a study of small shifts. The kinetic-energy part of a Hamiltonian for a two-body system may be rewritten in the center-of-mass frame as

$$\frac{1}{2m}(\mathbf{p}_1^2+\mathbf{p}_2^2)+\frac{1}{2M}(\mathbf{p}_1^2+\mathbf{p}_2^2)+\frac{\mathbf{p}_1\cdot\mathbf{p}_2}{M}, \tag{8}$$

where $\mathbf{p}_1$ and $\mathbf{p}_2$ are the momenta of the two electrons, m is the electron mass, and M is the mass of the nucleus. The first two terms combined can be accounted for by a rescaling of energies according to the appropriate reduced mass, $E_M = E_\infty M/(M+m)$, where E_∞ is the energy for infinite nuclear mass. The last term in expression 8, often called the specific mass shift (or mass polarization), will reflect a possible momentum correlation between the two electrons. Its magnitude is thus a critical test of theoretical predictions. While a significant specific mass shift of 486 μeV has been calculated for the ${}^1S$ ground state of H^- by Drake [51], Lindroth *et al.* [27] have predicted specific mass shifts of the ${}_2\{0\}_3^-$ and ${}_2\{0\}_4^-$ resonances to only $\sim$10 μeV and $\sim$0.33 μeV, respectively. The experimentally observed shift in energy for both the ${}_2\{0\}_3^-$ and ${}_2\{0\}_4^-$ resonances of 3.4(2) meV in the present study is entirely consistent with the 3.2 meV found by simply rescaling the transition energies according to the reduced mass and by assuming that the specific mass shift of the ground state of D^- can be scaled from that of H^- by the nuclear mass ratio.

The comparatively small size of the specific mass shift for the excited states of $A=-$ symmetry compared to the states of $A=+$ symmetry (the specific mass shift of the ${}_2\{0\}_2^+$ resonance is predicted to be four times as large as the shift for the ${}_2\{0\}_3^-$ resonance [32]) may be understood from a qualitative analysis of the kinetic energy in Eq. (8). The $A=-$ states are characterized by the out-of-phase radial motion of the electrons. This means that when one electron is close to the nucleus (has large momentum) the other is far from the nucleus (has small momentum). While the second term in Eq. (8) always collects a large contribution from either $\mathbf{p}_1^2$ or $\mathbf{p}_2^2$, the last term will be significantly suppressed by the smaller of the two momenta. For the in-phase $A=+$ states, conversely, the approximately equal size of $\mathbf{p}_1$ and $\mathbf{p}_2$ may result in more equal contributions from the two terms and hence a larger relative effect of the specific mass shift. It should be noted that very recently, Rislove *et al.* [21,22] reported the observation of a specific mass shift of -2.4 ± 1.1 meV, with an additional possible systematic error of 0.8 meV, for the related ${}^1D^e$ resonance below the H($n=2$) threshold. This value is significantly larger than the $\sim$0.1 meV predicted by several theoretical calculations (see references in [21]).

D. Future perspectives: Momentum-spread reduction

Although the resolution of the present experimental technique has allowed a more accurate determination of resonance energies and the detection of the second member of the ${}_2\{0\}_m^-$ series, the resolution is still insufficient for addressing several important questions: First, the width of the ${}_2\{0\}_3^-$ Feshbach resonance has not been resolved. Second, the third member of the ${}_2\{0\}_m^-$ series will be barely observable above the background cross section. It will have a width which is reduced by another factor of $\sim$29, Eq. (7), and a peak cross section (at infinitely high resolution) comparable to the ${}_2\{0\}_4^-$ resonance. Since the peak signal for the ${}_2\{0\}_4^-$ resonance is determined by the resolution, the signal at the peak of the third resonance can be estimated to be only $\sim$5% above the background cross section. Third, it will be tedious to observe the small (10%) increase in the cross section which marks the $n=2$ threshold. The observation of this structure would provide a calibration of the effective photon energy for this particular ion-beam energy and thus facilitate absolute position measurements for resonances.

As discussed in Sec. III B, the main contribution to the photon-energy resolution is from the momentum spread of the ion beam. One of the benefits of applying the storage ring is the option of using momentum-spread reduction techniques. This is based on the long interaction times that allow the manipulation of a specific ensemble of ions before the experiment is initiated. Electron cooling is a proven technique for momentum-spread reduction of stored positive ions [52]. The technique is based on the merging of a magnetically guided electron beam with the ion beam. By matching the velocities of electrons and ions, the ions transfer momentum spread to the much lighter electrons. The application of electron cooling to negative ions has been less examined. Fundamentally, negative ions of course do not capture the cooling electrons, which is an advantage. More important, however, is the fact that due to the larger cross section for collisional destruction in the rest gas, negative ions have much shorter storage times, typically by an order of magnitude, than positive ions. This means that there is much less time to obtain an equilibrium situation with a cooled negative-ion beam than in the case of positive ions.

The ASTRID electron cooler has been applied to the 1.6-MeV D^- beam. The effect of the electron beam is determined by observing the Schottky signal from the ion beam. As a consequence of the much shorter storage times, a standard spectrum analyzer cannot be used for this purpose, since the frequency spectrum is changing on a sub-second time scale. Instead an RF mixer and a frequency generator (local oscillator) are applied to shift the Schottky signal to

the ~10 kHz regime. The mixed-down signal is sampled on a standard PC analog-to-digital converter following each injection and commercial fast-Fourier-transform routines are used to determine the time-varying frequency spectrum. Following proper alignment of the electron and ion beams, the effect of the electron beam is unfortunately not just to reduce the momentum spread and consequently the width of the Schottky spectrum, but also to cause large and time-dependent shifts in the central frequency. This is due to rest-gas atoms being ionized by the electron beam and the resulting positive ions being captured in the space-charge potential of the electrons. This trapping then partially cancels the space-charge potential and thus increases the kinetic energy of the electrons during interaction with the ion beam. Consequently, the ions are dragged to gradually higher velocities as this capture process proceeds. This process also takes place for positive ions, but within several seconds an equilibrium is obtained and the Schottky frequency becomes constant. For the negative-ion beam, however, this process lasts several storage times leading to very small ion currents and hence small signal levels for the experiment. In order to shorten the time to reach equilibrium, a small AC field transverse to the electron beam is applied that excites the radial motion of the trapped ions [53]. With this technique a narrow and stable Schottky peak 2.8 to 4.5 seconds after the cooler is turned on is observed. Unfortunately, the momentum distribution obtained so far is not a simple Gaussian, but rather a fairly narrow Gaussian (with a width corresponding to $\Delta p/p = 1\times10^{-4}$) sitting on a broader pedestal ($\Delta p/p = 9\times10^{-4}$) representing ~10% of the stored ions. Regarding only the narrow (cooled) part of the beam, the electron cooling provides an improvement in resolution by a factor of four. Future improvements beyond this preliminary limit are expected and it seems feasible to avoid the broad pedestal.

The photodetachment cross section in the vicinity of the ${}_2\{0\}_3^-$ resonance is measured during the application of electron cooling. The results, shown in Fig. 3, exhibit a peak which is roughly half as broad as that of Fig. 2(b). This reduction is smaller than the factor of four improvement in resolution measured in the Schottky spectra and is a signature of the contribution from the natural width of the resonance. Although the experimental points on Fig. 3 should be regarded as preliminary in the sense that they are obtained with a comparatively low photon flux (poor statistics) and with an uncooled component of the ion beam, the data have been attempted fitted to a Fano profile convolved with the experimental resolution as determined from the shape of the Schottky peaks. The low statistics in the tail of the resonance exclude a determination of the asymmetry parameter q, but by applying a value in the interval -30 to -10 (as determined experimentally above, Sec. IV A), the width can be determined to be 57(15) μ eV, with the uncertainty representing only the statistical spread. This number is (within the quoted uncertainty) independent of the choice for q inside the above interval. The width obtained with the cooled beam is consistent with the determination of Sec. IV A, but appears to be slightly higher than the most recent theoretical predictions, c.f. Table I. A reinvestigation of the ${}_2\{0\}_3^-$ resonance with better resolution and higher photon flux is scheduled for the near future. An improved result should be able to destinguish between the various theoretical results for the width (see Table I).

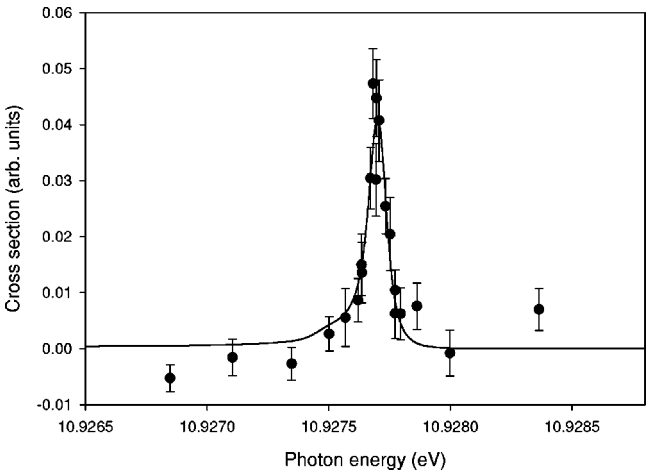

FIG. 3. Relative photodetachment cross section vs. effective photon energy for the region near the ${}_2\{0\}_3^-$ Feshbach resonance after the application of electron cooling. The points are experimental data while the solid curve represents the best fit to a Fano profile convolved with the experimental resolution determined from the Schottky-frequency measurement, as discussed in the text. The error bars indicate a statistical uncertainty of one standard deviation.

As mentioned in the introduction, the Bryant group has contributed an enormous amount of information about ${}^1P$ resonances in the negative hydrogen ion. Their technique was very versatile for a large photon-energy range. The improved resolution provided by the present technique has proven useful for the study of very narrow structures in the photodetachment cross section and it seems an obvious extension of the present studies to examine the $A=-$ series of resonances below H($n=3$), which went undetected in the previous studies. The resolution of the present technique is, however, dependent on the ion-beam energy needed to obtain the required effective photon energy. It follows from Eq. (4) that an increased beam energy leads to a poorer resolution. For instance, in order to obtain an effective photon energy corresponding to the $n=3$ threshold, the beam will need a kinetic energy of 19.4 MeV (H^-), which would reduce the resolution from the present 180 μeV to 1.7 meV. This certainly allows an improved-resolution investigation of the $A=+$ series below the $n=3$ threshold, where two members have already been observed [8,14]. The resolution does not, however, permit studies of the narrow (and weaker) $A=-$ resonances below $n=3$. These resonances should appear as strongly asymmetric Fano profiles ($q\sim1$) and with the resolution above would only modulate the signal by ~2% (for the ${}_3\{0\}_4^-$ and ${}_3\{0\}_5^-$ ${}^1P^0$ resonances, based on parameters from [32]). As a consequence, the study of higher-lying resonances also requires the application of momentum-spread-reduction techniques. The resonances are, however, also fairly weak, but if the resolution is improved by a factor of ~10, the two $A=-$ resonances discussed above would give a >10% modulation and could be observed by collecting data for long periods. The observation

of members of another $A=-$ series would be a strong test of theoretical predictions.

V. CONCLUSION

Although seemingly the most simple negative ion, the spectrum of H^- is still not fully explored. Gains in the experimental knowledge of the system are closely linked to on-going technical developments. On the theoretical side, the new experimental abilities immediately prompt a reinvestigation of the structure of the system. For instance, the truncation of the dipole series due to the relativistic splitting of the $n=2$ threshold was pointed out already by Gailitis and Damburg [49], but due to the extremely large basis needed to describe the highly-excited states, it is only through modern computational approaches that the precise behavior can be predicted [27,33]. At the time of publication of our first experimental results [23], little attention had been paid to the higher-lying members of the $A=-$ series. Since then the situation has changed and it seems the next major contribution should be made by experiment. The preliminary studies presented in this paper indicate how this may be obtained through the use of momentum-spread reduction techniques.

ACKNOWLEDGMENTS

We would like to acknowledge the invaluable assistance of the ASTRID staff and from the electron-cooler group. H. K. Haugen and P. Kristensen were important contributors during early stages of this experiment. This work was supported by the Danish National Research Foundation through the Aarhus Center for Atomic Physics (ACAP). One of us (P.B.) gratefully acknowledges the support of the Carlsberg Foundation.

[1] R.P. Madden and K. Codling, Phys. Rev. Lett. **10**, 516 (1963).
[2] S.J. Buckman and C.W. Clark, Rev. Mod. Phys. **66**, 539 (1994).
[3] A.R.P. Rau, J. Astrophys. Astron. **17**, 113 (1996).
[4] H.C. Bryant and M. Halka, in *Coulomb Interactions in Nuclear and Atomic Few-Body Collisions*, edited by. F.S. Levin and D.A. Micha (Plenum Press, New York 1996).
[5] H. Massey, *Negative Ions* (Cambridge University Press, Cambridge, England, 1976).
[6] H.C. Bryant *et al.*, Phys. Rev. Lett. **38**, 228 (1977).
[7] P.A.M. Gram *et al.*, Phys. Rev. Lett. **40**, 107 (1978).
[8] M.E. Hamm *et al.*, Phys. Rev. Lett. **43**, 1715 (1979).
[9] H.C. Bryant *et al.*, in *Atomic Physics 7*, edited by D. Kleppner and F.M. Pipkin (Plenum, New York, 1981).
[10] H.C. Bryant *et al.*, Phys. Rev. A **27**, 2889 (1983).
[11] D.W. MacArthur *et al.*, Phys. Rev. A **32**, 1921 (1985).
[12] P.G. Harris *et al.*, Phys. Rev. Lett. **65**, 309 (1990).
[13] P.G. Harris *et al.*, Phys. Rev. A **42**, 6443 (1990).
[14] M. Halka *et al.*, Phys. Rev. A **44**, 6127 (1991).
[15] M. Halka *et al.*, Phys. Rev. A **46**, 6942 (1992).
[16] J.T. Broad and W.P. Reinhardt, Phys. Rev. A **14**, 2159 (1976).
[17] H.R. Sadeghpour and C.H. Greene, Phys. Rev. Lett. **65**, 313 (1990).
[18] H.R. Sadeghpour, Phys. Rev. A **43**, 5821 (1991).
[19] H.R. Sadeghpour, C.H. Greene, and M. Cavagnero, Phys. Rev. A **45**, 1587 (1992).
[20] A. Stinz, Phys. Rev. Lett. **75**, 2924 (1995).
[21] D.C. Rislove *et al.*, Phys. Rev. A **58**, 1889 (1998).
[22] D.C. Rislove *et al.*, Phys. Rev. A **59**, 906 (1999).
[23] P. Balling *et al.*, Phys. Rev. Lett. **77**, 2905 (1996).
[24] H.H. Andersen *et al.*, Phys. Rev. Lett. **79**, 4770 (1997).
[25] U. Fano, Rep. Prog. Phys. **46**, 97 (1983).
[26] C.D. Lin, Adv. At. Mol. Phys. **22**, 77 (1986).
[27] E. Lindroth, A. Bürgers, and N. Brandefelt, Phys. Rev. A **57**, R685 (1998); private communication.
[28] D.R. Herrick and O. Sinanoglu, Phys. Rev. A **11**, 97 (1975).
[29] O. Sinanoglu and D.R. Herrick, J. Chem. Phys. **62**, 886 (1975).
[30] Y.K. Ho, Chin. J. Phys. **29**, 327 (1991).
[31] J. Tang *et al.*, Phys. Rev. A **49**, 1021 (1994).
[32] E. Lindroth, Phys. Rev. A **52**, 2737 (1995).
[33] A. Bürgers and E. Lindroth (unpublished).
[34] T. Purr, H. Friedrich, and A.T. Stelbovics, Phys. Rev. A **57**, 308 (1998).
[35] T. Purr and H. Friedrich, Phys. Rev. A **57**, 4279 (1998).
[36] M-K. Chen, J. Phys. B **30**, 1669 (1997).
[37] T.T. Gien, J. Phys. B **31**, L1001 (1998).
[38] W.H. Kuan, T.F. Jiang, and K.T. Chung, Phys. Rev. A **60**, 364 (1999).
[39] S.M. Hooker and C.E. Webb, Prog. Quantum Electron. **18**, 227 (1994).
[40] J.F. Reintjes, *Nonlinear Optical Parametric Processes in Liquids and Gases* (Academic Press, Orlando, 1984).
[41] C.R. Vidal, in *Tunable Lasers*, edited by L.F. Mollenauer, J.C. White, and C.R. Pollock (Springer-Verlag, Berlin, 1992).
[42] A.H. Kung, J.F. Young, and S.E. Harris, Appl. Phys. Lett. **22**, 301 (1973).
[43] R. Mahon, T.J. McIlrath, V.P. Myerscough, and D.W. Koopman, IEEE J. Quantum Electron. **15**, 444 (1979).
[44] L.J. Zych and J.F. Yong, IEEE J. Quantum Electron. **14**, 147 (1978).
[45] J.A.R. Samson, *Techniques of Vacuum Ultraviolet Spectroscopy* (John Wiley & Sons, New York, 1967).
[46] S.L. Kaufman, Opt. Commun. **17**, 309 (1976).
[47] S.P. Møller, in *Proceedings of the IEEE Particle Accelerator Conference*, edited by S. T. Corneliussen (IEEE, Piscataway, NJ, 1993).
[48] S.P. Møller, private communication.
[49] M. Gailitis and R. Damburg, Zh. Éksp. Teor. Phys. **44**, 1644 (1963) [Sov. Phys. JETP **17**, 1107 (1963)].
[50] D.R. Herrick, Phys. Rev. A **12**, 413 (1975).
[51] G.W.F. Drake, Nucl. Instrum. Methods B **31**, 7 (1988).
[52] H. Poth, Phys. Rep. **196**, 135 (1990).
[53] J. Marriner, D. Möhl, Y. Orlov, S. Van der Meer, and A. Poncet, Part. Accel. **30-31**, 971 (1990).